COMPDYN 2011
III ECCOMAS Thematic Conference on
Computational Methods in Structural Dynamics and Earthquake Engineering
M. Papadrakakis, M. Fragiadakis, V. Plevris (eds.)
Corfu, Greece, 26–28 May 2011

EXPERIMENTAL AND NUMERICAL STUDY OF THE BEHAVIOUR OF HIGH DISSIPATION METALLIC DEVICES FOR THE STRENGTHENING OF EXISTING STRUCTURES

A.A. Karalis[1], K.A. Georgiadi-Stefanidi[2], T.N. Salonikios[3], K.C. Stylianidis[1] and E.S. Mistakidis[2]

[1] Dept. of Civil Engineering, Aristotle University of Thessaloniki
52124, Thessaloniki, Greece
kcstyl@civil.auth.gr

[2] Dept. of Civil Engineering, University of Thessaly,
Pedion Areos, 38334 Volos, Greece
emistaki@uth.gr

[3] Institute of Engineering Seismology and Earthquake Engineering,
Thessaloniki, Greece
salonikios@itsak.gr

Keywords: Strengthening, Existing Structures, Experimental and Numerical Study, High Dissipation Metallic Devices.

Abstract. *The use of steel bracing systems for the strengthening of existing reinforced concrete (RC) frames may lead to increase of both strength and stiffness. However, in most of the cases the main target is the increase of the energy dissipation capacity. This paper studies, both experimentally and numerically, the efficiency of a specific strengthening type which utilizes a small steel link element having an I-shaped cross-section connected to the RC frame through bracing elements. The energy is dissipated through the plastification of the steel link element. The case studied in this paper is a typical one bay, single storey RC frame constructed according to older code provisions, which is strengthened through two different types of steel link elements. The behaviour of the strengthened frames is studied with respect to the one of the original bare frame. The experimental study is supported by complete numerical simulations of the performed tests. To this end, detailed numerical models are formulated, which are able to follow the highly non-linear nature of the problem, involving the plastification of the steel rebars, the cracking and plastification of concrete and the plastic deformation and hysteretic response of the dissipative link elements.*

1 INTRODUCTION

The strengthening of existing reinforced concrete (RC) buildings with pilotis (soft ground floor) is a current necessity in seismic prone areas. It is well known that the majority of these buildings were designed and built according to older codes. Moreover, they lack sufficient longitudinal and transverse reinforcement and their structural materials are of low quality or exhibit degradation of their mechanical properties. As a result, these structures present weaknesses concerning their strength, ductility and stiffness. Strengthening this type of structures is essential in order to avoid damages or even loss of life from earthquakes.

One of the more popular methods for the strengthening of RC frames is the use of steel braces. A specific category in this strengthening type concerns the additional use of dissipative devices which exhibit extensive plastification under the design earthquake. During the last decades significant research effort has been dedicated in this direction. For example, RC frames strengthened with such system were tested by Kunisue et al [1]. Failure was observed at the elastoplastic energy dampers. The test results showed that the strength and the energy dissipation capacity can be significantly improved by the use of these dampers. A calculation method was also suggested for the estimation of the strength increase in strengthened RC frames and satisfactory approximation between experimental and analytical results was observed. In tests performed by Perera et al [2] the strengthening of masonry infilled RC frames was examined. In some frames the masonry was replaced by a system of two steel braces and significant improvement of the energy dissipation was observed. Tests on two full scale, four storey RC frames were executed by Pinto et al [3]. For the frame with no strengthening interventions high vulnerability to seismic loads was observed. It was found that through the use of steel braces, the seismic response of the strengthened frame and the energy dissipation capacity are significantly improved. A full scale, 3D, two storey, RC frame was tested by Antonucci et al [4]. Viscous dampers were used at the connection point of the top of the bracing system to the middle of the RC beam. It was found that viscous dampers can dissipate up to 95% of the induced seismic energy. The storey drift was also significantly reduced. Three tests were performed by D'Aniello [5] on an existing RC building that was strengthened against seismic actions by the use of the same system of two steel braces. It was concluded from the tests that shear elements can be easily connected at the concrete and the steel elements and can also be easily replaced after an important seismic event. A simplified simulation method was also used and a satisfactory approximation resulted between analytical and experimental results. It is concluded from the literature review that the use of a system of two steel braces with a purposely designed steel link element at the top with shear and/or flexural type of failure, could increase the shear strength and the energy dissipation capacity of existing RC frames under seismic actions.

In the present work the efficiency of a specific type of strengthening device, which consists of two steel braces connected to the RC frame through two different types of dissipative steel link elements, is investigated. Six specimens were tested under horizontal cyclic loading, three of them (one bare RC frame and two similar strengthened RC frames) without additional vertical loads at the columns and another identical group of three specimens with vertical loads.

The experimental investigation is complemented by a numerical study. All the tested RC frames are simulated numerically through detailed finite element (F.E.) models, which are able to follow the highly non-linear nature of the problem [6, 7, 8]. The numerical results are then compared with the respective experimental ones. After the verification of the simulation models according to the experimental results, it will be possible to perform reliable "numeri-

cal tests" in order to investigate the effects of several parameters, reducing the required number of experiments [9].

2 TYPES OF RC FRAMES STUDIED

2.1 Geometry and configurations

The specimens studied in this paper represent a single storey one bay frame rigidly based on a strong foundation and are manufactured to a scale of 1:3. The RC part is exactly the same in all the tested specimens. The geometry and the reinforcement arrangement of the specimens are shown in Fig. 1.

The frames are assumed to be constructed according to older regulations and thus, smooth steel rebars and sparsely spaced stirrups were used, even at the critical regions of the possible plastic hinges. Moreover, the anchorage length of the steel bars was small and does not meet the modern requirements.

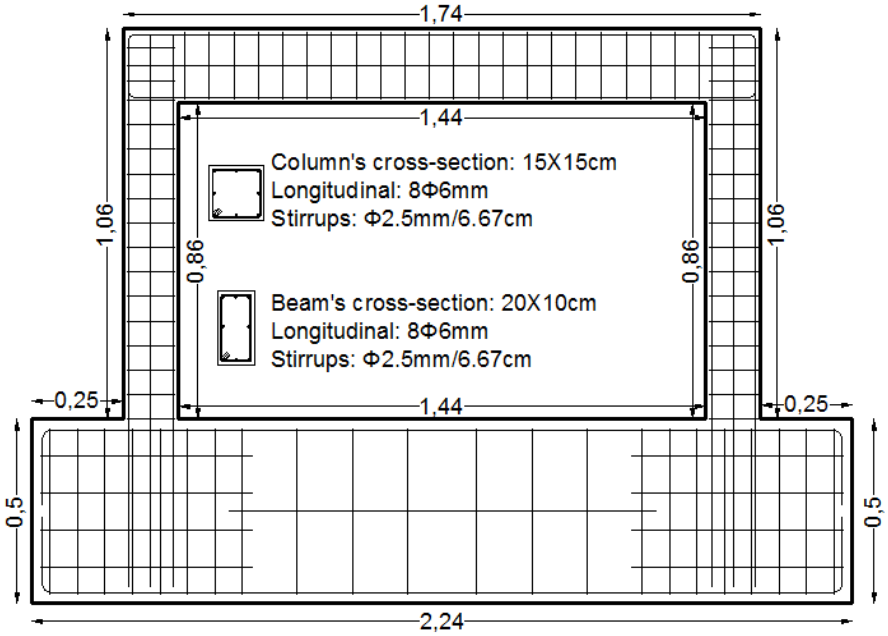

Figure 1: Geometry and reinforcement arrangement of the specimens (m).

The presented frame is strengthened by means of a steel link which is connected to the beam of the RC frame and to strong steel bracing members. As shown in Fig. 2, the bracing system is composed by two steel elements that are connected to each other at their top. At this point there is a steel plate on which the link element is welded. The top of the link element is connected to the midpoint of the beam through a steel U shaped collar which is placed around the beam. The collar element is connected to the top beam by means of six bolts which pass through the width of the cross-section of the beam. The diagonal elements of the bracing system were connected at the lower ends of the columns and on the base beam by external threaded rods. The elements of the bracing system, the collar and the connections to the beams and the columns were not considered as parameters under investigation in the present study. Therefore, they were overdesigned in order to avoid local failures at these elements. Consequently, the inelastic deformations of the strengthened specimens are expected to be concentrated mainly at the link element. This type of link elements is expected to significantly increase the strength and stiffness of the strengthened frame. However, the most important

advantage of these systems is the high energy dissipation capacity and, consequently, the reduction of the seismic strength demands.

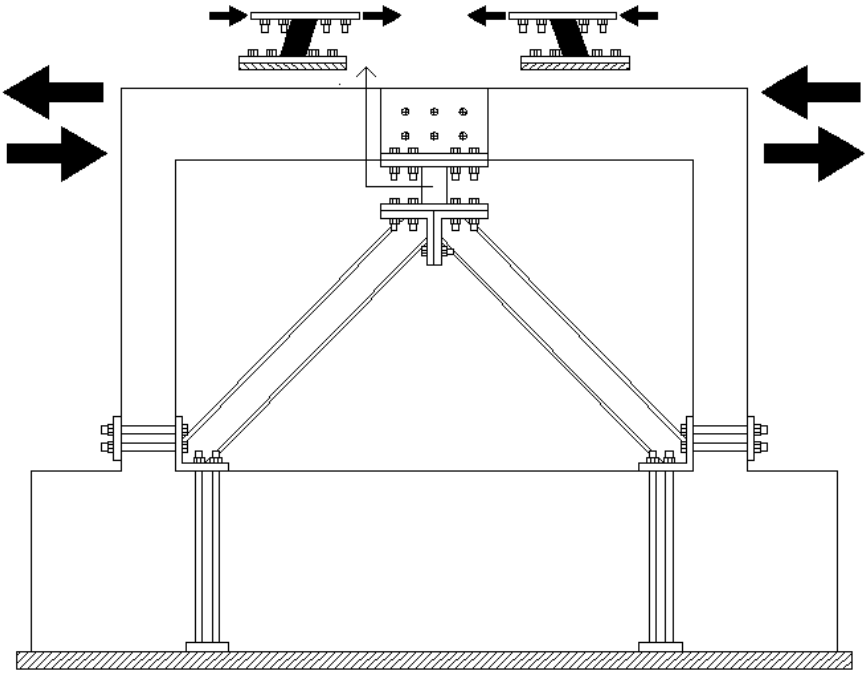

Figure 2: Specimens F2 and F3 strengthened by steel bracing system and a steel link element at the top.

Three different types of specimens were tested. Specimen type F1 is the bare frame, which is used as a reference for the evaluation of the strengthening types. In order to allow the direct comparison, the bracing system was also installed in this frame (as in the other specimens) but without the link element. This layout was selected in order to ensure the same geometrical conditions for all the specimens concerning the free height of the columns.

In the other two types of specimens (types F2 and F3) the bracing system was connected in the middle of the top beam by a steel link element. The links used in each type are presented in Fig. 3. The first link, used in the type F2 specimens, is a steel element that has a symmetrical I cross-section with total section height d = 60 mm, flange width b = 30 mm, flange and web thickness t = 6 mm and length l = 100 mm. The second link, used in the type F3 specimens, has also a symmetrical I cross-section with total section height d = 80 mm, flange width b = 40 mm, flange and web thickness t = 6 mm and length l = 200 mm.

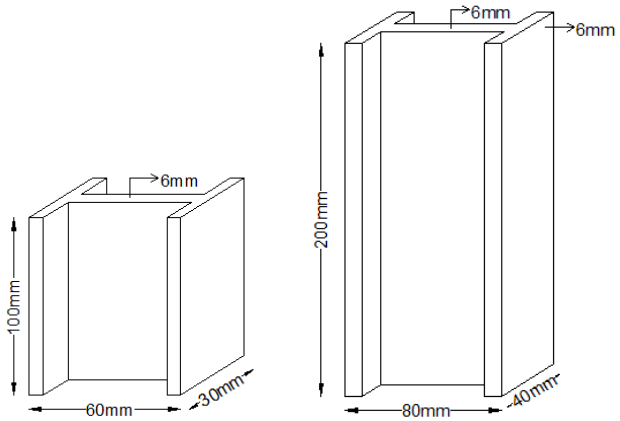

Figure 3: The dissipative steel link elements of the strengthened frames F2 and F3, respectively.

The above three types of specimens (F1, F2 and F3) were tested with and without additional vertical loading placed at the columns. Therefore, the total number of specimens and tests was six. The three specimen types in which the vertical loading was present at the columns during the testing are referenced as F1,N, F2,N and F3,N respectively. The tests are presented schematically in Figs 4 - 6.

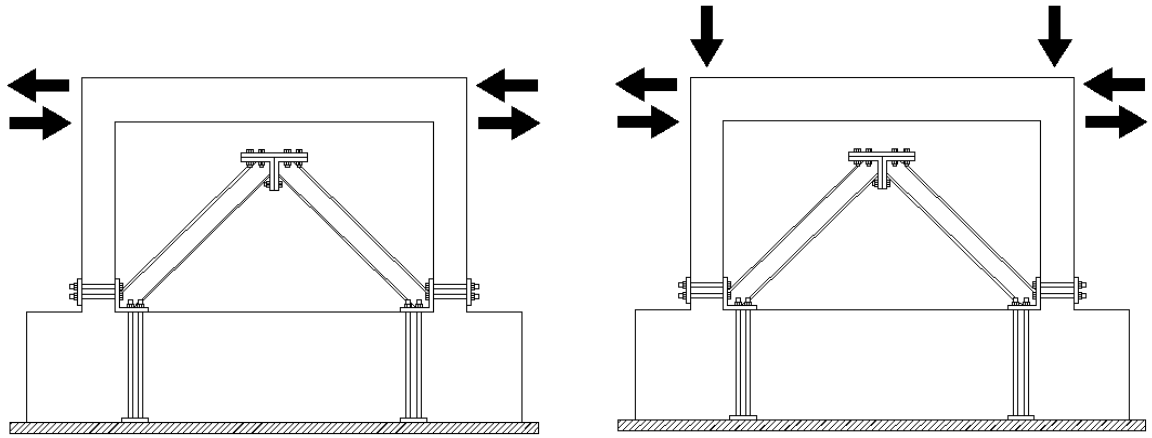

Figure 4: Specimen F1 and F1,N with the bracing system of the strengthened frames but without a link element

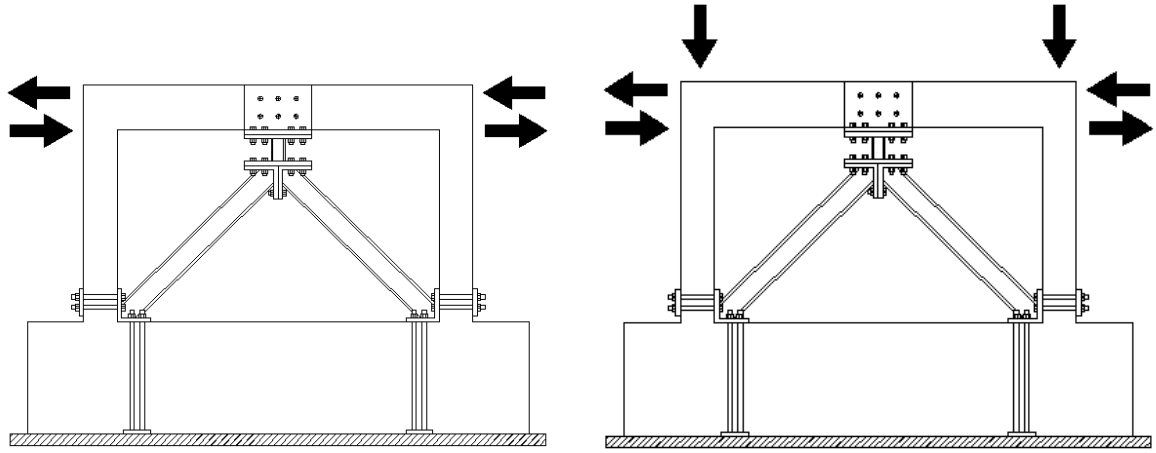

Figure 5: Specimens F2 and F2,N strengthened by steel bracing system and a steel link element at the top.

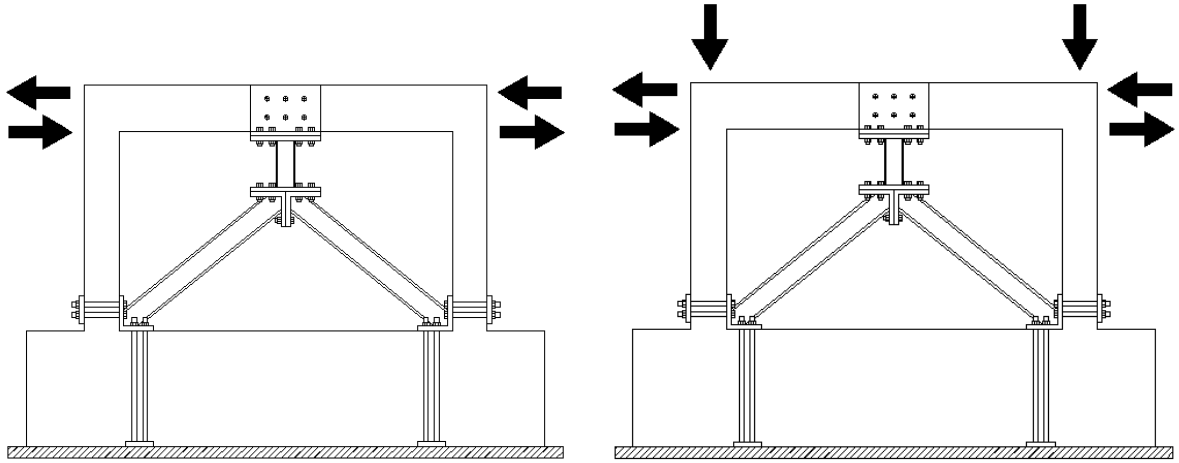

Figure 6: Specimens F3 and F3,N strengthened by steel bracing system and a steel link element at the top.

2.2 Materials

As the RC specimens were assumed to be constructed according to older regulations, a low strength concrete was used with a compressive strength of 16 MPa and a tensile strength of 2.1 MPa. The smooth steel rebars of the longitudinal reinforcement had a yield stress of 450 MPa and an ultimate stress of 540 MPa (it was not possible to find lower strength smooth steel rebars with a diameter of 6 mm), while the transverse reinforcement had a yield stress of 265 MPa and an ultimate stress of 390 MPa. Finally, the yield stress of the steel link elements was equal to 300 MPa and the ultimate stress equal to 375 MPa.

2.3 Experimental test setup

For the tests, the facilities of the Laboratory of Concrete and Masonry Structures of the Aristotle University of Thessaloniki, were used (Fig. 7). The reaction frame consists of steel beams and columns connected to each other by prestressed threaded rods. One double acting actuator is connected at the top beam of the specimens applying horizontal displacement reversals. Another actuator can also be connected to the system to apply vertical axial loads on the columns through a top steel beam in a load control mode.

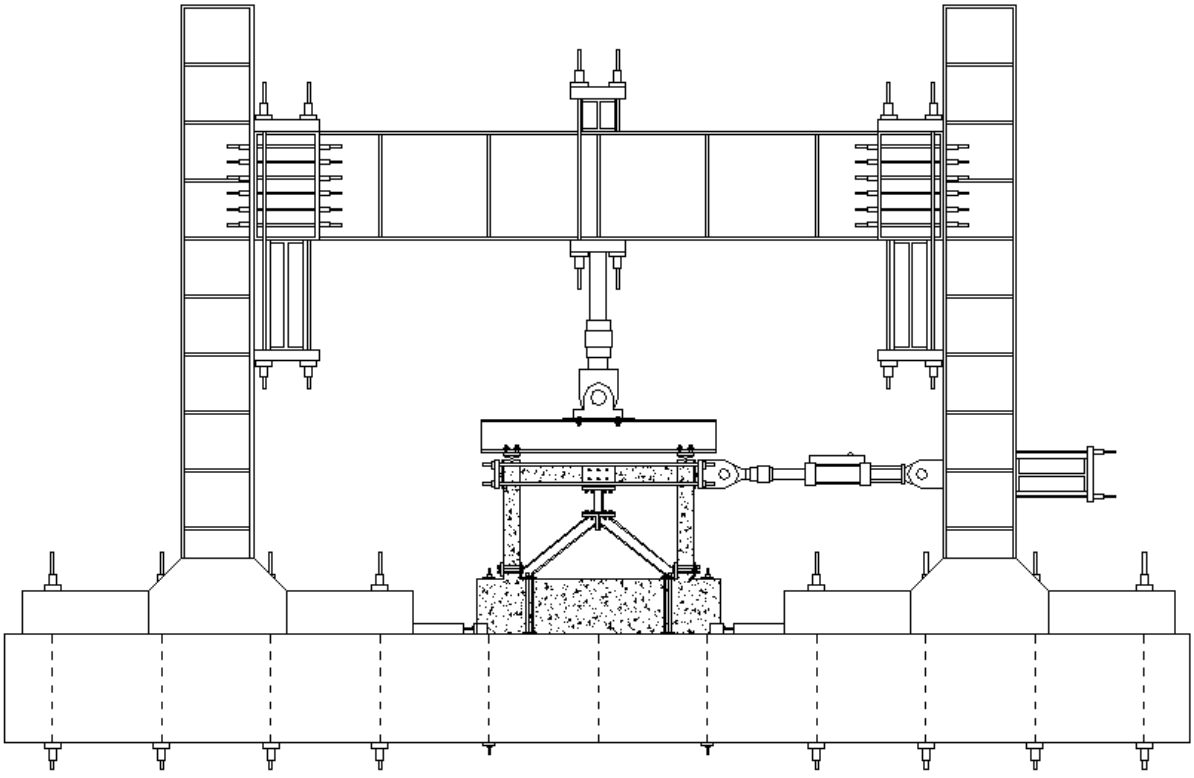

Figure 7: Test setup

The reaction frame is connected to the strong floor of the laboratory by the use of steel stoppers in combination with vertical prestressed threaded rods. The test specimens were also connected to the floor by the same technique. It is worth mentioning that during the tests no slip was recorded between the specimens and the laboratory floor. The horizontal actuator was connected at the top of the specimens by a system of two stiff steel plates at the vertical outer sides of the beam - column joints, connected to each other by four long threaded rods. In order to allow free rotation at the connection points, beyond the 3D rotational hinges of the actuator at the ends of its length, two more rotational hinges were provided between the steel plates and the two top beam - column joints of each specimen.

2.4 Loading procedures

The horizontal loads were imposed in a displacement control mode. The displacement history was composed by 16 levels of displacement. For each displacement level, two full cycles were imposed. The loading increment had the value of 1mm until a total displacement of 3mm and the value of 3mm till the maximum displacement (42mm). For the specimens with the axial loading (F1,N – F2,N – F3,N), apart from the horizontal displacement, a constant axial load of 80kN was applied at each column. Figure 8 shows the horizontal loading history.

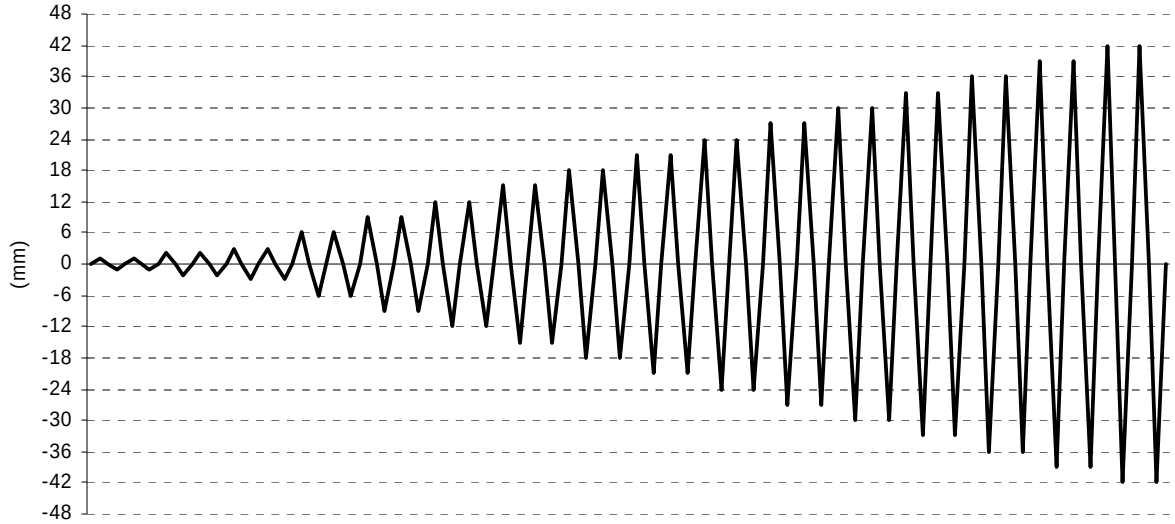

Figure 8: Horizontal loading history

The specimens were instrumented by the use of seven LVDTs. The layout of these instruments is shown in Fig. 9. LVDTs 1, 5, 2, 6 were used for the measurement of the shortening and the elongation of the outer fibres at the ends of the left column. LVDT 8 was used for the measurement of the top horizontal displacement of the specimen and was compared with the measurements of the internal LVDT of the horizontal actuator. LVDTs 4 and 7 were used for the measurement of the net horizontal displacement at the top and bottom ends of the steel link element. The measurements of the external and internal LVDTs together with the measurements given by the load shell of the horizontal actuator were recorded through a digital controller. In the present work, only a small part of the experimental measurements and the post-processed data are presented due to limited available space.

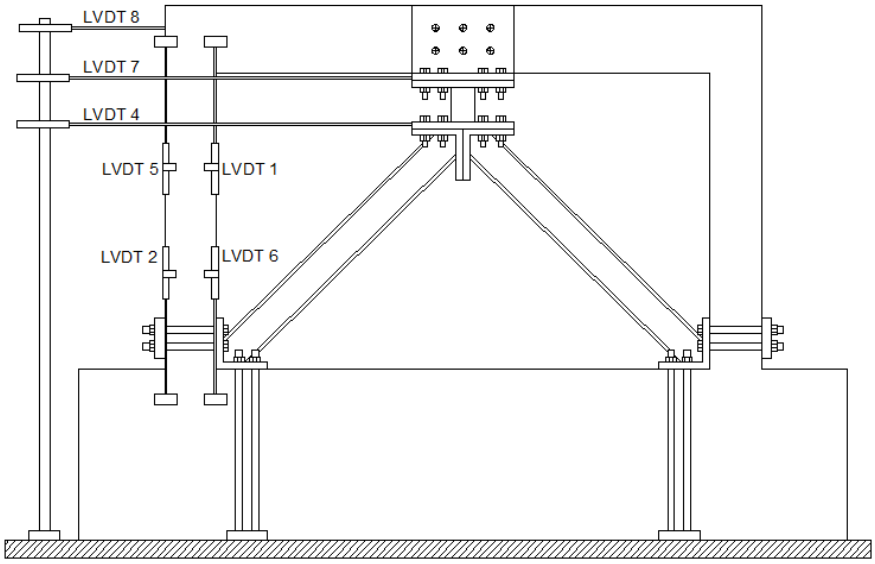

Figure 9: LVDT arrangement on the specimens

3 THE PRINCIPLES OF NUMERICAL SIMULATION

The numerical simulation of the tested frames presented several difficulties due to the complexity of the problem and the existence of various nonlinearities, such as cracking in concrete and the plastification of the steel link elements. Moreover, while a three-dimensional model is expected to be more realistic and reliable due to the nature of its elements, it has the disadvantage of a high computational cost. Therefore, simpler two-dimensional models were formulated, which were able to capture in a rather accurate manner the overall behaviour of the studied problem [10]. The attempt to simulate a 3D problem through a 2D finite element model resulted in several simulation problems, which had to be solved efficiently.

3.1 Geometric and material properties

The 2D simulation models of the RC frames consist of different F.E. meshes, which overlap, connected at the same grid of nodes. Especially for the models of the strengthened F2 and F3 frames, another F.E. mesh was added to the F.E. mesh of the RC frame, simulating the link element. Plane-stress and truss elements were used for the formulation of the 2D numerical models. Figure 10 shows the numerical model of the F2 strengthened frame together with a detail of the link element, after the discretization. The plane-stress elements were used for the simulation of the concrete and of the steel link elements. The truss elements were used for the simulation of the longitudinal and transverse reinforcement. The properties of the problem in the third direction (perpendicular to the modelling plane) were taken into account by assigning different thickness values to the respective finite elements.

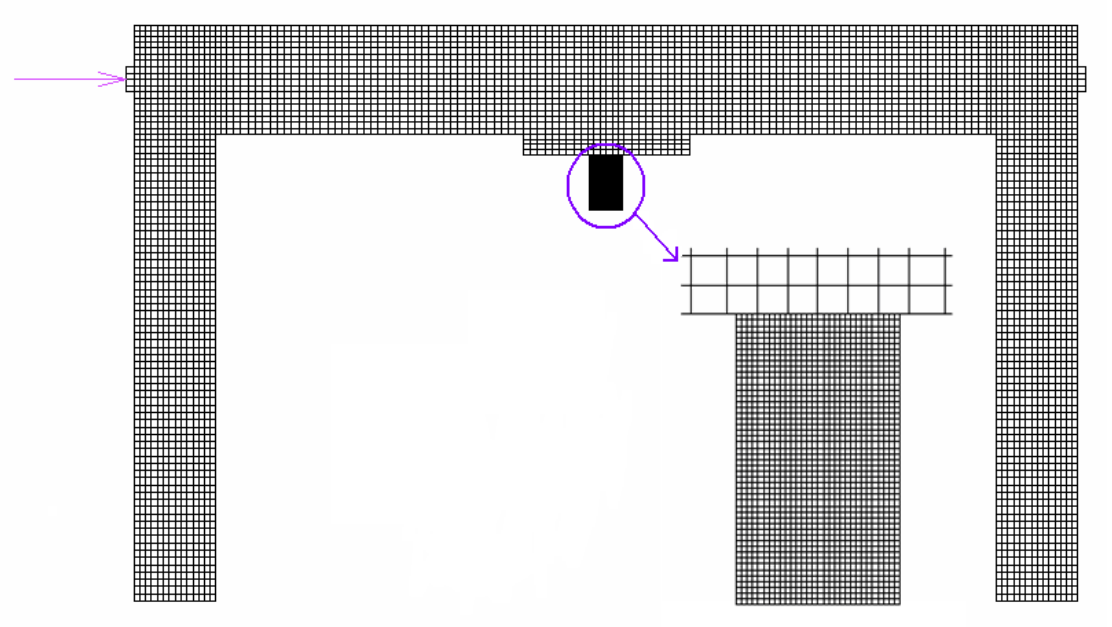

Figure 10: The 2D F.E. model of the strengthened RC frame and detail of the steel link element.

The plane-stress elements representing the concrete beam and columns were assigned a thickness equal to the width of the corresponding cross-section, that is 100 mm and 150 mm thickness for the beam and the columns, respectively. The cross-sectional area of the two-node, constant cross-section truss elements that represent the longitudinal and transverse reinforcement was taken equal to the total area of the corresponding reinforcing bars. That is, for the line of elements representing the top and the bottom steel reinforcement the cross-sectional area was $3\times28.26=84.78$ mm^2 (3Ø6) and for those representing the middle longitudinal reinforcement, the cross-sectional area was $2\times28.26=56.52$ mm^2 (2Ø6). For the lines of elements representing the stirrups of the beam and columns, the cross-sectional area was $2\times4.91=9.81$ mm^2 in order to account for the two vertical legs of the Ø2.5 stirrup. For the steel links, the plane-stress elements representing the flanges and those representing the web were assigned different thickness values. More specifically, for the first link (F2) the elements representing its web were assigned a thickness of 6 mm and those representing the flanges were assigned a thickness of 30 mm, whereas for the second link (F3), the elements representing the web had thickness equal to 6 mm and those representing the flanges had thickness equal to 40 mm.

It must be noted that the links were simulated through a much denser finite element mesh, as already shown in Fig. 10. This dense discretization of the links was considered necessary in order to simulate as accurately as possible their behaviour, which dominates the strengthened systems. The two different F.E. meshes (the one corresponding to the RC frame and the one representing the link element) were connected through kinematical relationships, due to the fact that their nodes, at their common boundary, do not coincide.

Figure 11 presents the stress-strain relationship considered for concrete, steel reinforcement and the steel links. The elements representing concrete were equipped with the stress-strain relationship of Fig 11a, which exhibits an elasto-plastic behaviour for compressive loading and a cracking behaviour for tensile loading. The loss of tensile strength after cracking was modelled through a softening branch with a slope $k_s=10^8$ MPa. The elasticity modulus was taken equal to 28.4 GPa and the Poisson's ratio $\nu = 0.16$. The longitudinal and transverse reinforcement bars were assumed to behave elastoplastically with hardening. A modulus of elasticity of 200 GPa and a Poisson's ratio $\nu = 0.20$ were given. The stress-strain diagram for

the steel rebars is depicted in Fig. 11b. Finally, the F.E. simulating the steel links were also equipped with the stress-strain relationship given in Fig.11b, which exhibits elastoplastic behaviour with hardening. The elasticity modulus for these elements was taken equal to 210 GPa and the Poisson's ratio $v = 0.30$.

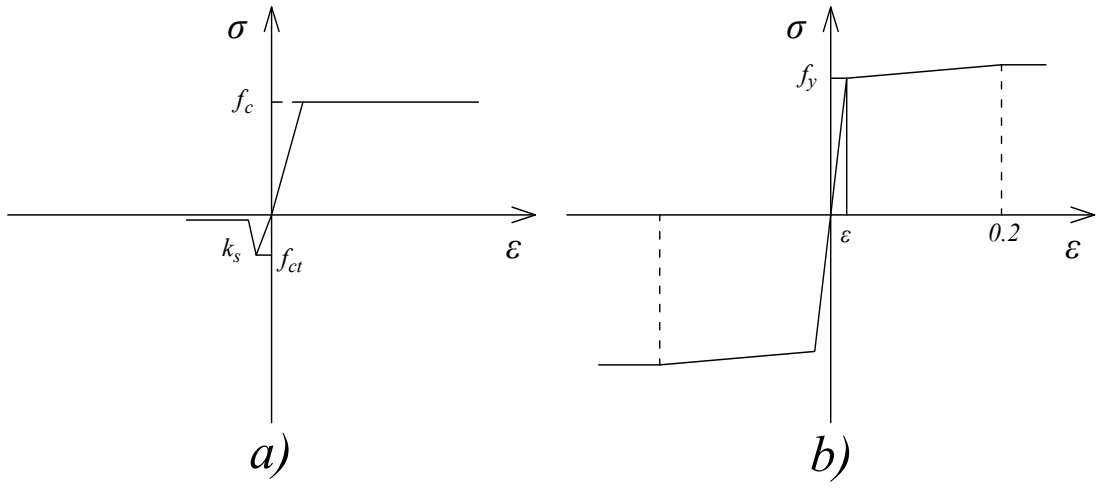

Figure 11: Stress-strain relationships considered for a) concrete and b) all the steel elements of the model.

3.2 Boundary conditions – loading procedure

All the specimens (F1, F2 and F3) were subjected to horizontal cyclic loading, with and without additional vertical load at the columns. The cyclic load was applied incrementally in the form of induced displacement, whereas the constant vertical load was applied as a point load. The simulation of the load application procedure introduced several difficulties, which required a special numerical treatment. In general, it was not possible to apply the load directly to a nodal point of the F.E. mesh, due to the elastic-plastic and cracking properties of concrete. When the applied load caused the formation of a compressive stress zone in the neighbourhood of the load application node, stress concentrations and non-realistic stress fields occurred, creating excessive plastification of the elements representing concrete. In order to avoid this phenomenon, a steel plate was placed on each load application position, through which the respective load was applied.

On the other hand, during the load reversal, the applied load produced a tensile stress zone in the region of the applied load. Even for moderate load values, stress concentration appeared locally, near the node at which the load was applied and therefore, non-realistic conditions for cracking were created, destroying the adjacent elements and leading to the premature termination of the numerical process. To overcome this obstacle, a system of two plates was adopted, one on the upper left and one on the upper right side of the frame. Unilateral contact conditions were assumed between the plates and the frame. The two plates were connected by kinematical constraints in order to achieve the load application in both directions and so that only compressive forces are imposed through the respective contact surfaces of the specimen. The above described loading procedures resulted in rather realistic stress and strain fields in the load application areas.

Finally, clamped supports were assumed at the positions where the steel rigid braces are connected to the frame and to the steel link.

3.3 Numerical solution procedure

The solution to the described numerical problem was obtained by using the software code MSC-MARC. A Newton-Raphson iterative procedure was applied to handle the nonlinearities of the problem. The cyclic load was applied in the form of an induced displacement δ and the resulting force P at the points of the incrementally applied displacement was monitored. A relative convergence criterion was adopted, based on the residual forces. The relative force tolerance was set to 0.01.

4 EXPERIMENTAL AND NUMERICAL RESULTS

4.1 Overall behavior of the specimens

Figures 12-14 present the load – displacement curves of the tested specimens. Also, in Fig. 15, the envelop curves that result from the aforementioned diagrams (consideration of first cycles only) are compared. In Fig. 16 the dissipated energy with respect to the imposed displacement for each specimen is presented. The observations on the response of the specimens during the tests and the obtained results are given below.

Specimen F1: During the first cycles, flexural cracks were formed, initially at the base and later at the top of the columns. The cracks at the base of the columns were formed just over the point where the Λ-shaped steel bracing system connects at the columns (Fig. 17). At these cracks the reinforcement was elongated inelastically and thus, flexural plastic hinges were formed. The inelastic deformations were all developed at these plastic hinges. Although the stirrups were sparsely spaced, the strength of the specimen appeared a slight increase, even for drifts of the order of 3% (Fig. 12). For higher levels of the imposed displacement, strength reduction was observed.

Specimen F1,N: It can be noticed, even from the first cycles of the imposed load, that the stiffness of this specimen is higher than the stiffness of the corresponding specimen without the axial force (F1). Moreover, the hysteresis loops of the F1,N specimen are richer than those obtained from the F1 frame. Initially, cracks appeared at the columns and at the two ends of the top beam. As the values of the imposed cyclic displacement increased, the inelastic deformations were mainly developed at the plastic hinges which were formed at the ends of the columns. Due to the existence of the axial loads at the columns, the strength of the specimen and the dissipated energy were increased by 50% and 100% respectively, in comparison with specimen F1 (Figs 15 and 16).

Specimen F2: In this case, due to the activation of the steel link, there was a significant increase of the strength, the stiffness and the energy dissipation capacity of the specimen, in comparison with the bare frames (Figs 13, 15 and 16). More specifically, the strength of the F2 specimen was four times higher than that of the F1 specimen. Also, the hysteresis loops were very rich and no pinching occurred. The link started to fail by fracture at the tensioned regions of the link, for a drift of 1.8%. As the loading was cyclic, the fracture appeared at both ends of the link (Fig. 18). The welds did not show signs of failure. After the failure of the link element, the overall behaviour of the F2 frame, in terms of strength and energy dissipation capacity, appeared to be similar to the behaviour of the F1 frame. The final failure mode was similar as in the case of the specimen F1, since the plastic hinges were formed at the same locations.

By the use of the U-shaped steel jacket, the force undertaken by the link element was transferred at the middle of the beam. Due to this reason, many cracks appeared at the middle of the top beam, as well as, loss of concrete cover (Fig. 19). However, the crack pattern at the

ends of the columns and at the ends of the beam didn't differ from those that appeared in specimen F1. Moreover, after the failure of the link element the response of the two specimens was very similar.

Specimen F2,N: Due to the existence of the axial load, the strength and stiffness of this specimen were increased, in comparison with the specimen F2 (Figs 13 and 15). Moreover, this specimen appears to have an increased strength and dissipation capacity of the order of 40% and 50% respectively with respect to that of the specimen F2 (Figs 15 and 16). The failure mode of the link element was the same as in the previous case. The link failed again for a drift of 1.8%. After the failure of the link element, the recorded response of the specimen F2,N was similar with the response of the specimen F1,N.

Specimen F3: This specimen was strengthened with a link element of different type (Fig. 3). The dimensions of the cross-section of the present link in combination with its longer length resulted in lower stiffness compared to the link of the specimen F2. However, the ultimate strength for this specimen is slightly higher than that of specimen F2. The main improvement for the present specimen is that the strength was sustained without reduction until a drift of 2.7%, thus, improving the ductility of the strengthened frame (Figs 14 and 15). The failure of the link element started at a drift of 2.7% and completed at a drift of 3.6%. After that point the specimen had the response of the unstrengthened specimen F1. This high ductility of the specimen is attributed to the higher rotational capacity of the link element. Due to the higher forces and the significant inelastic deformations that were developed, the U-shaped jacket at the middle of the top beam caused local damage. Moreover, the bending moment that develops at the mid-span of the beam due to the eccentricity of the horizontal force undertaken by the link, led to the development of high shear forces along the two parts of the beam. Characteristic is the development of bidiagonal shear cracks at the left and right parts of the top beam (Fig. 20). Also, plastic hinges were formed at both ends of the columns.

Specimen F3,N: Due to the existence of the axial loads at the columns, the strength of the specimen and the dissipated energy were increased by 35% and 40% respectively, in comparison with specimen F3 (Figs 15 and 16). For an imposed displacement of 3mm, the resisted force was 90kN. Due to the high stiffness, the first cracks appeared at the top beam, at the left and right of the U-shaped jacket. Also, due to the existence of axial loads, the cracks at the columns were significantly reduced. For this reason, the inelastic deformation was developed mostly at the middle of the top beam through the rotation of the U-shaped jacket. The ultimate strength was achieved for an imposed displacement of 21mm. Due to the extended damage that developed at the top beam, the test was terminated at that displacement value, for safety reasons. The link element did not fail.

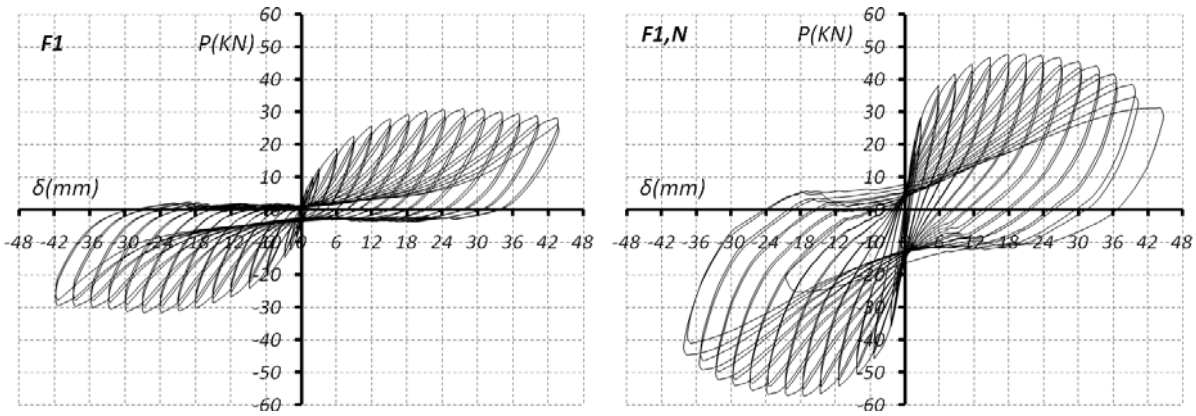

Figure 12: Load – displacement (P-δ) curves of the frame F1 and F1,N

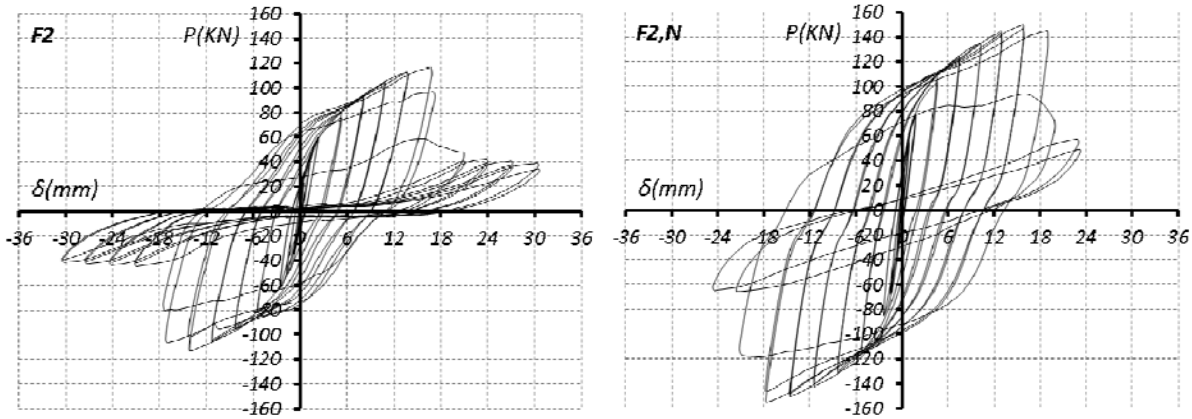

Figure 13: Load – displacement (P-δ) curves of the frame F2 and F2,N

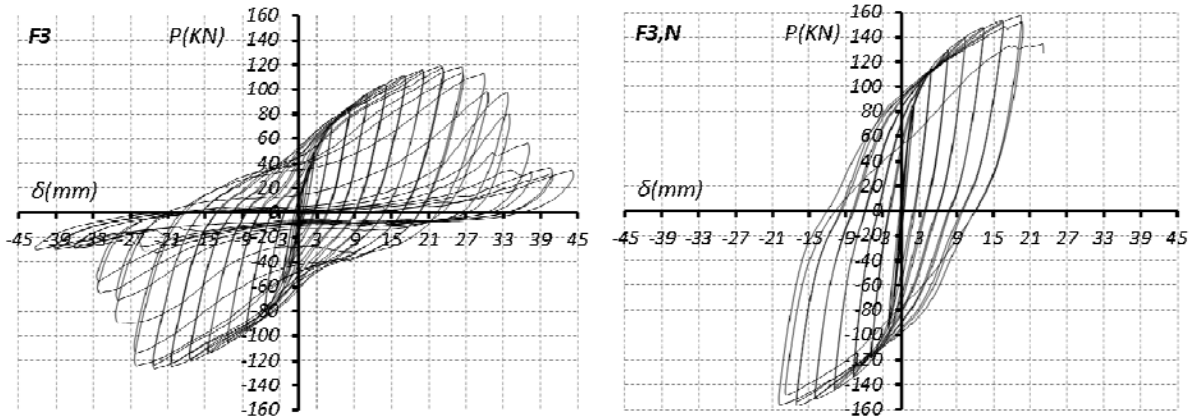

Figure 14: Load – displacement (P-δ) curves of the frame F3 and F3,N

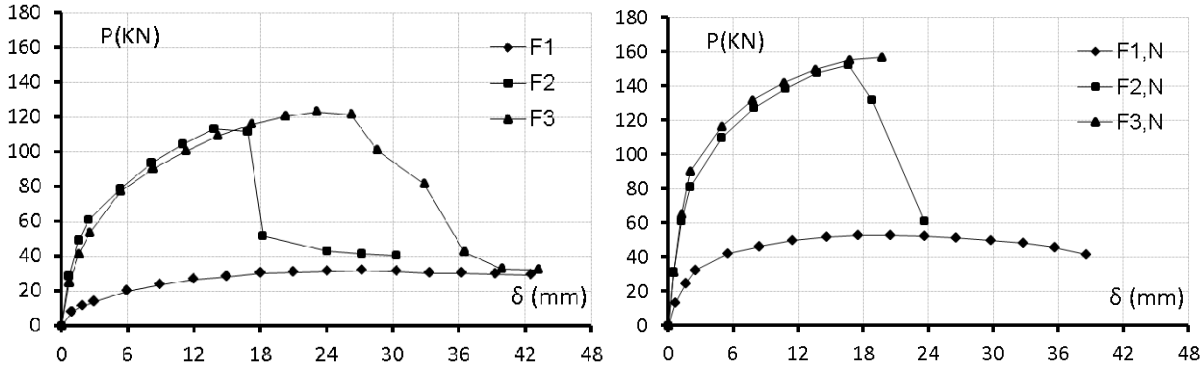

Figure 15: Comparison of load – displacement (P – δ) envelopes (first cycles only)

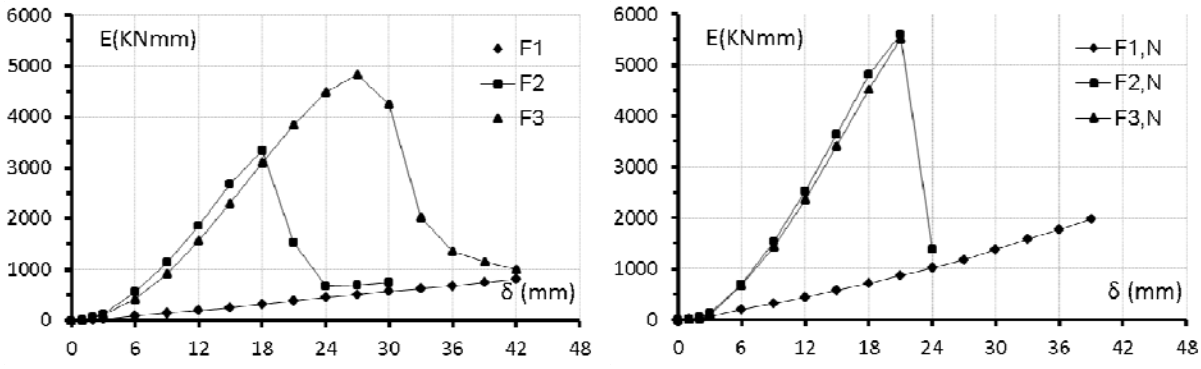

Figure 16: Comparison of energy dissipation – displacement (E – δ) envelopes (first cycles only)

Figure 17: Plastic hinge at the bottom of the column (F1)

Figure 18: Failure mode of the link element (F2)

Figure 19: Concrete cover failure (F2)

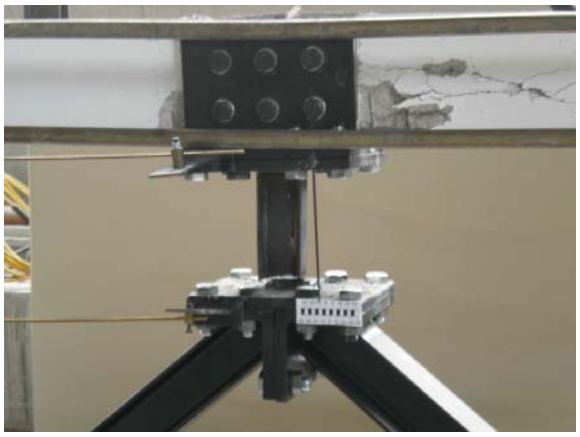

Figure 20: Cracks at the middle of the top beam (F3)

4.2 Overall behaviour of the specimens

Before displaying the numerically obtained results, it should be mentioned that, for most of the cases treated here, it was not possible to simulate the performed experiments beyond a displacement of about 12 mm, due to numerical instabilities in the models which led to the termination of the applied Newton – Raphson iterative procedure. The reason for the aforementioned problem was the significant damage of concrete that occurred for displacement values higher than 12 mm. For the same reason it was decided to simulate numerically only one load cycle for each displacement level instead of two similar cycles that were applied in the experiments. Therefore, the experimental P-δ curves used in this section for the comparison of the numerical with the experimental results are actually, part of the complete response diagrams of each experiment (Figs. 12-14).

The comparison between the numerical and experimental P-δ curves of the bare frame without axial force (F1) and with axial force (F1,N) is presented in Fig. 21. It can be noticed that the numerical model cannot approximate adequately the unloading branch of the experimental P-δ diagram, leading to narrower hysteresis loops. It seems that the smeared crack approach used for the modelling of cracking cannot simulate accurately enough the closure of cracks and therefore, the behaviour of the specimen during the load reversal procedure. This deficiency of the numerical model is more obvious in the case of F1,N, where, except from the narrower hysteresis loops, one can notice differences between the load values P obtained

for the negative cycles by the analysis and the experiment. Figure 22 presents the comparison of the P-δ envelopes obtained by the experiment and the analysis of the F1 and the F1,N frames. In these diagrams, only positive values are given for each applied displacement level, that correspond to the mean of the absolute values of the respective positive and negative cycles. The aforementioned discrepancies that appear in the P-δ diagrams of the F1,N case concerning the experimental and numerical load values of the negative cycles, are reflected in the respective P-δ envelope curves. Figure 23 gives the comparison of the dissipated energy in each load cycle. It can be observed that for the case of F1 the differences between the experimental and numerical values of dissipated energy are rather small and result from the narrower numerical hysteresis loops. However, for the case of the F1,N frame, the corresponding discrepancy is much wider, due to the additional differences in the negative load values.

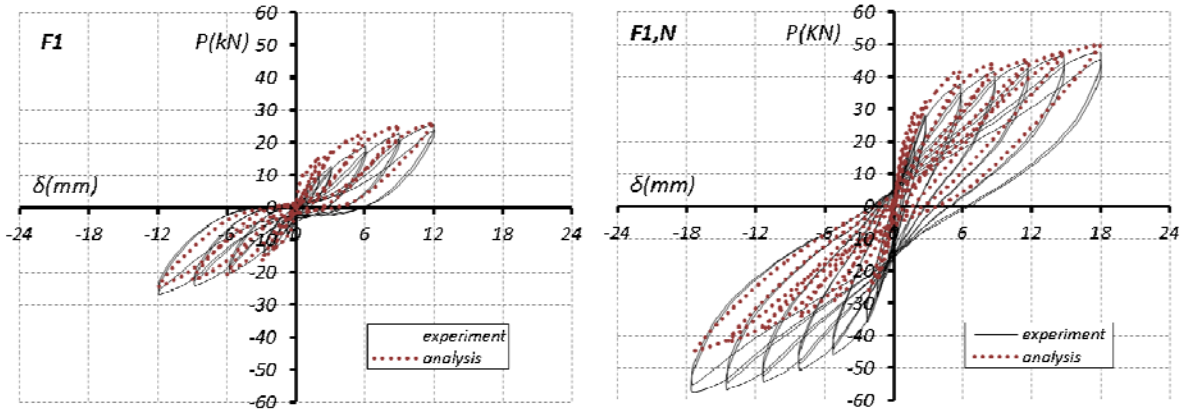

Figure 21: Comparison of the numerical and experimental results of the frames F1 and F1,N.

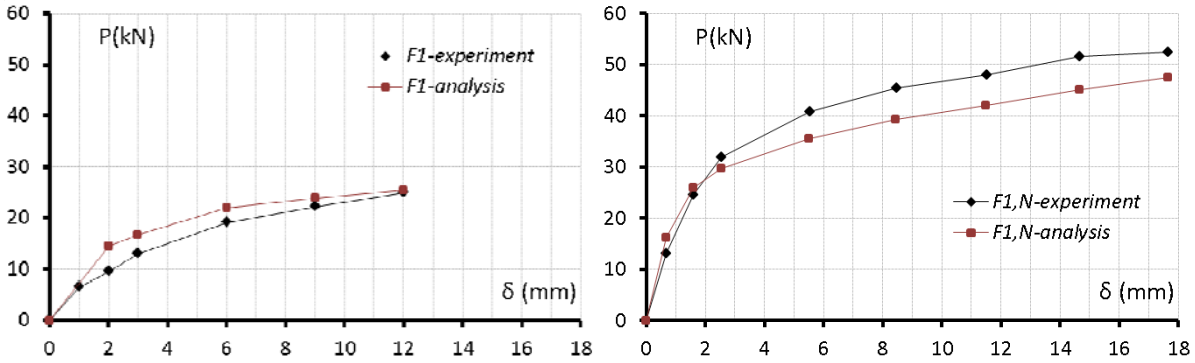

Figure 22: Comparison of the P-δ envelope results obtained by the experiment and the analysis of the frames F1 and F1,N.

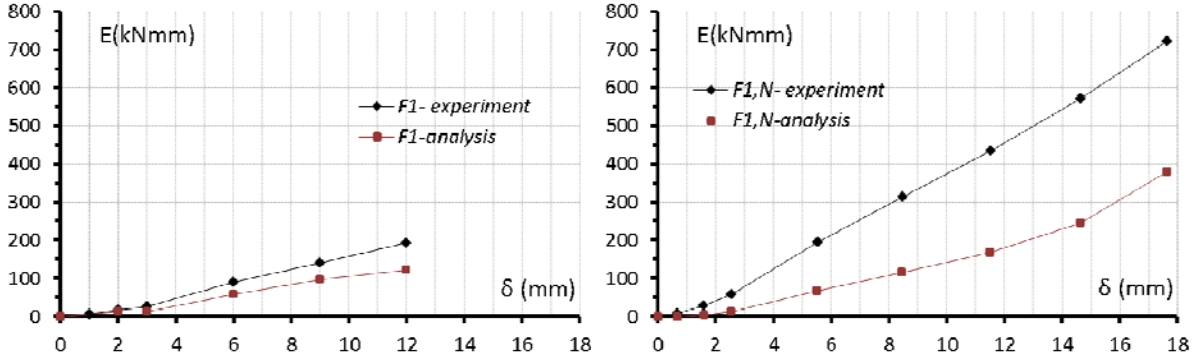

Figure 23: Comparison of the experimental and the numerical results for the dissipated energy in the frames F1 and F1,N.

Contrary to the bare frame F1, the overall behaviour of the frames strengthened by the steel link elements, F2 and F3, is significantly improved after the immediate activation of the link elements. Figure 24 shows the P-δ curves for the F2 strengthened frame (without axial load) and the F2,N strengthened frame (with axial load), obtained by the 2D numerical model together with the experimental results. Figure 25 displays the corresponding envelopes of the P-δ curves. It is noticed that, especially for the case of the F2 frame, there is a good agreement between the numerical and the experimental results, as far as the load values, the quality of the hysteresis loops and therefore, the overall behaviour of the specimen, is concerned. The small differences that arise in the obtained values can be considered acceptable, taking into account the highly nonlinear nature of the studied problem. However, once again, in the case where the axial load is imposed at the columns, greater differences can be noticed between the numerical and the experimental results, mainly in terms of the obtained load values, whereas the quality of the hysteresis loops is similar. In Fig. 26 the numerical and experimental results for the dissipated energy of the F2 and F2,N frames are presented. As expected, there is a very good agreement between the results for the F2 frame, whereas some differences arise for the F2,N strengthened frame, due to the above mentioned differences in the obtained values of the P-δ curves.

The same conclusions can be drawn from the comparison of the numerical and experimental results presented in Figs 27, 28 and 29, which concern the F3 strengthened frame (without axial load) and the F3,N strengthened frame (with axial load). For the F3 case, the numerical and experimental results are in a rather good agreement, in terms of obtained load values, quality of the hysteresis loops and dissipated energy. For the F3,N case, although the numerical P-δ curves, the P-δ envelope curves and the dissipated energy present some differences with respect to the experimentally obtained ones, they can be considered acceptable, taking into account the nonlinear phenomena that are present in the physical model.

It can be concluded that the good agreement between the numerical and experimental results of the strengthened frames is derived from the fact that in these cases the behaviour of the steel link element is dominant. In this case, the numerical model has the ability to simulate efficiently the isotropic and homogenous behaviour of the steel link element, as well as its stable elasto-plastic deformation.

Finally, Figs 30 and 31 show the plastic strain fields of the link elements F2, F2,N and F3, F3,N, respectively for a displacement of about 12 mm. Both types of links present a combined shear and bending behaviour. However, their failure is mainly of bending type, as greater stresses appear in the flanges at the top and bottom ends of the elements, rather than the web, especially in the case of the F3 and F3,N links. The failure modes match well with the failure type of the link elements that was noticed in the corresponding experiments.

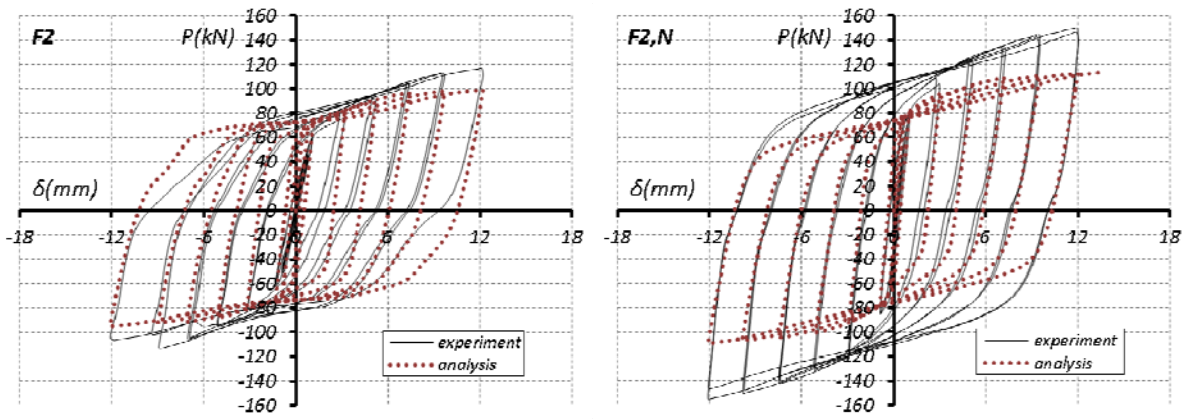

Figure 24: Comparison of the numerical and experimental results of the frames F2 and F2,N.

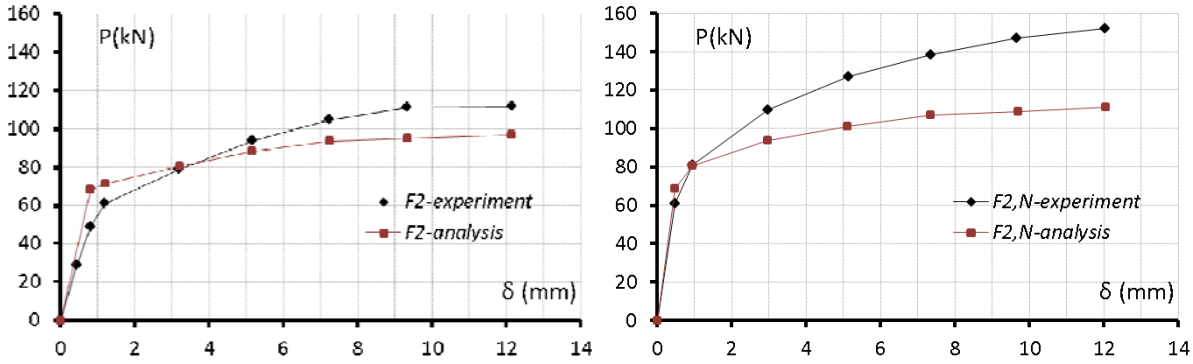

Figure 25: Comparison of the P-δ envelope results obtained by the experiment and the analysis of the frames F2 and F2,N.

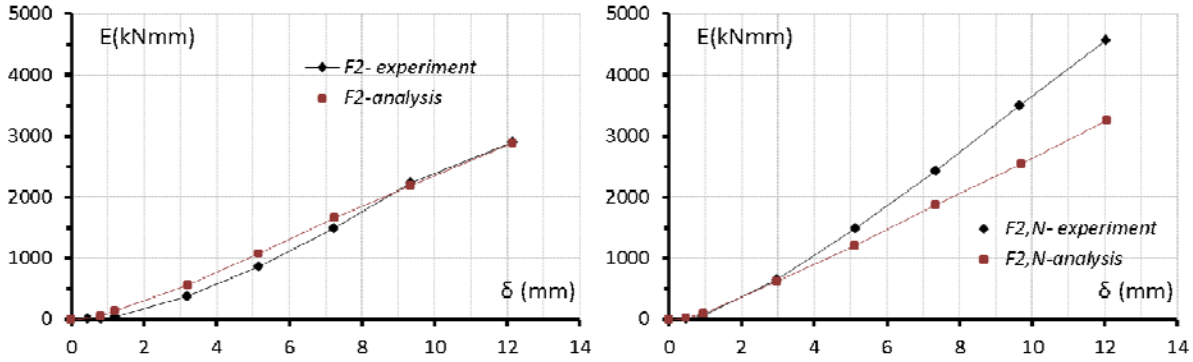

Figure 26: Comparison experimental and the numerical results for the dissipated energy in the frames F2 and F2,N.

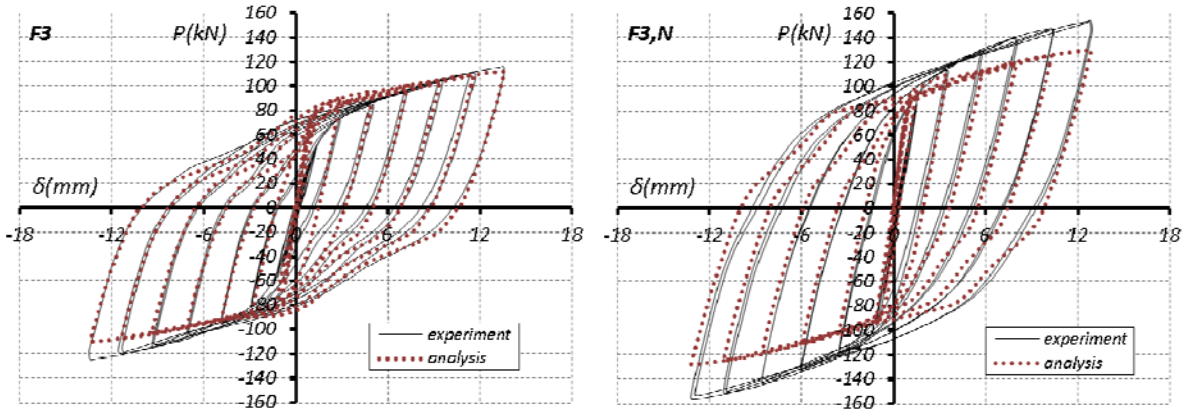

Figure 27: Comparison of the numerical and experimental results of the frames F3 and F3,N

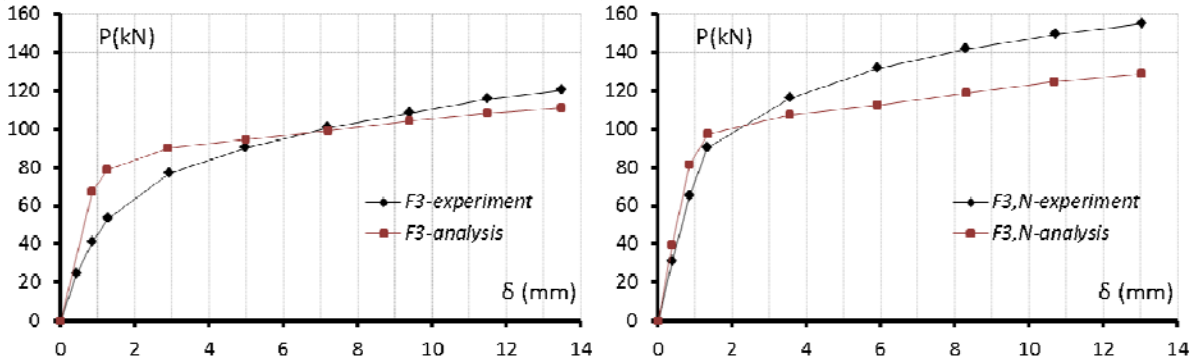

Figure 28: Comparison of the P-δ envelope results obtained by the experiment and the analysis of the frames F3 and F3,N.

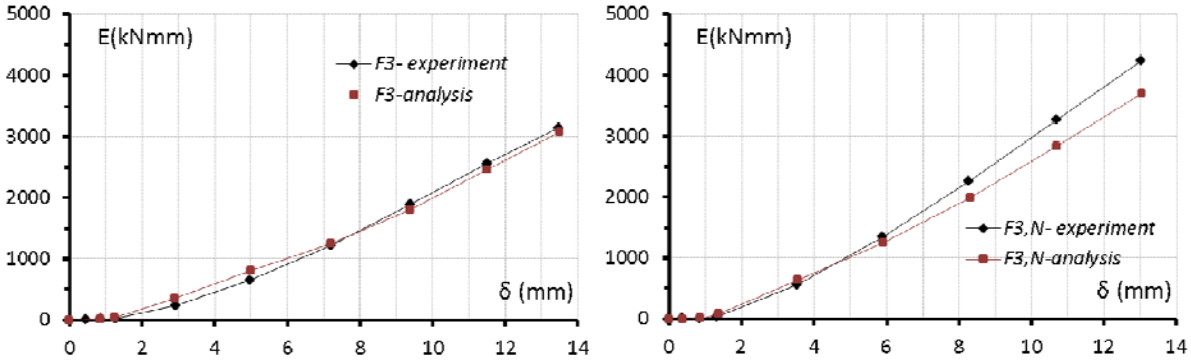

Figure 29: Comparison of experimental and the numerical results for the dissipated energy in the frames F3 and F3,N.

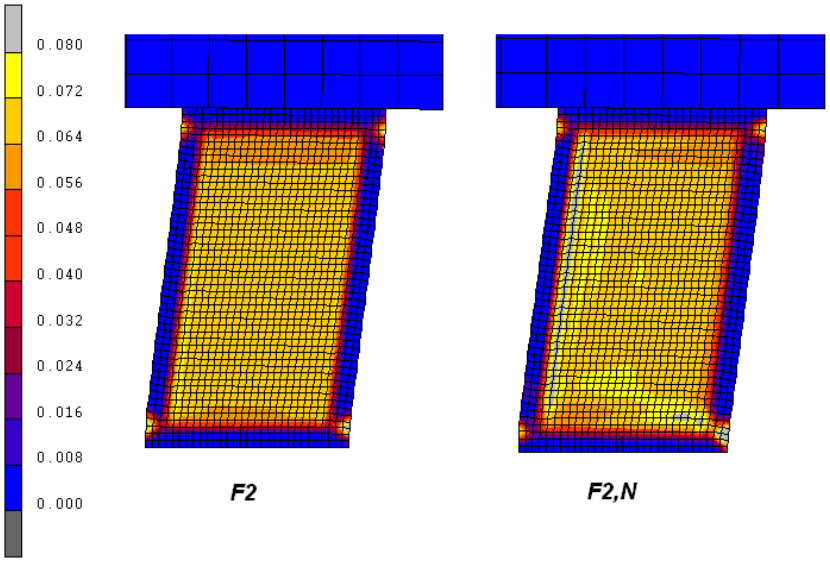

Figure 30: Plastic strain of the steel link elements of the frames F2 and F2,N, for a displacement of 12mm.

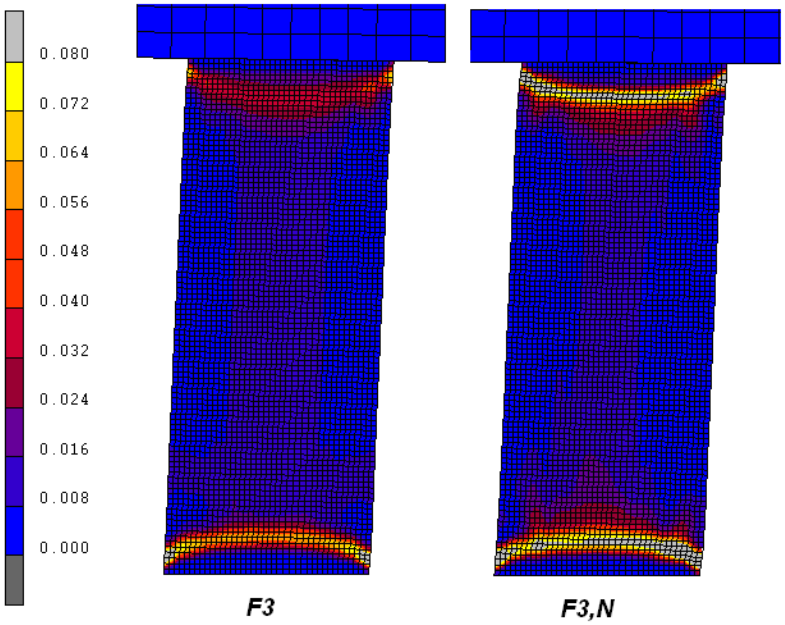

Figure 31: Plastic strains of the steel link elements of the frames F3 and F3,N, for a displacement of 12mm.

5 CONCLUSIONS

After comparing the behaviour of the specimens under study, it can be concluded that the use of the steel link elements can increase considerably the strength, the stiffness, but mainly the energy dissipation capacity of the frame. Moreover, the use of the F3 type of link element results to slightly lower overall stiffness, but to increased ultimate strength, with respect to the F2 type of link element. However, the significant improvement for the F3 strengthened frame is its increased ductility; the high load carrying capacity is maintained without reduction for much higher values of imposed displacements. Also, it is evident that the existence of axial loads at the columns resulted to an increase of the strength, stiffness and dissipated energy for all the frames studied. It must be noted, however, that attention should be paid to the connection of the link element to the midpoint of the beam, through the U-shaped steel jacket, as local damage appeared at that specific area of the beam of the strengthened frames. By a careful selection of the geometry of the steel link and appropriate detailing of its connection with the frame, this local failure at the middle of the top beam can be prevented, so that it does not affect or alter the failure mode of the frame.

Finally, after the comparison of the numerical with the experimental results, some differences are observed in the case of the bare frames (F1 and F1,N) which are attributed to the inability of the used type of finite elements to simulate adequately the unloading behaviour of concrete. On the other hand, the results obtained from the numerical models of the strengthened frames can be considered satisfactory in terms of the stiffness, load carrying capacity, quality of the hysterisis loops and dissipated energy, with respect to the experimental results, given the complexity of the studied problem.

ACKNOWLEDGEMENTS

The work presented here is part of a broader program, partially sponsored by the Greek Earthquake Planning and Protection Organization, the contribution of which is gratefully acknowledged.

REFERENCES

[1] A. Kunisue, N. Koshika, Y. Kurokawa, N. Suzuki, J. Agami, M. Sakamoto, Retrofitting method of existing reinforced concrete buildings using elasto-plastic steel dampers. *12WCEE*, New Zealand, 2000.

[2] R. Perera, S. Gomez, E. Alarcon, Experimental and analytical study of masonry infill reinforced concrete frames retrofitted with steel braces. *Journal of structural Engineering, ASCE,* **130**, 2032-2039, 2004.

[3] A. Pinto, F. Taucer, Assessment and retrofit of full scale models of existing rc frames. S.T. Wasti, G. Ozcebe eds. *Advances in Earthquake Engineering for Urban Risk Reduction,* Springer Netherlands, 353-367, 2006.

[4] Antonucci, R., Balducci, F., Bartera, F., Castellano, M. & Chaudat, T. 2006. Shaking table test on rc frame braced with fluid viscus dampers. *1st European Conference on Earthquake Engineering and Seismology (1st ECEES)*, Switzerland, 3-8 Semptember 2006. paper#650.

[5] M. D'Anielo, Seismic upgrading of rc structure by steel eccentric bracing (Experimental and numerical study. *Pollac Periodica,* **1**, 17-32, 2006.

[6] A. Abdollahi, Numerical strategies in the application of the FEM to RC structures. *Computers and Structures,* **58**, 1171-1182, 1996.

[7] T. Rabczul, J. Akkermann, J. Eibl, A numerical model for reinforced concrete structures. *International Journal of Solids and Structures,* **42**, 1327-1354, 2005.

[8] C.Y. Wang, H.Y. Ho, R.Z. Wang, H.H. Huang, Numerical simulations of non-ductile RC frames with infilled brick panel under cyclic loading. *Journal of the Chinese Institute of Engineers,* **31**, 827-840, 2008.

[9] D.A. Nethercot, The importance of combining experimental and numerical study in advancing structural engineering understanding. *Journal of Constructional Steel Research,* **58**, 1283-1296, 2002.

[10] K. Georgiadi-Stefanidi, E. Mistakidis, P. Perdikaris, T. Papatheocharis, Numerical simulation of tested reinforced concrete beams strengthened by thin fibre-reinforced cementitious matrix jackets. *Earthquakes and Structures,* **1**, 345-370, 2010.